Effect of steady-state hydrogen coverage on the evolution of crosshatch morphology during $Si_{1-x}Ge_x/Si(001)$ growth from hydride precursors

T. Spila,[a] P. Desjardins,[b] J. D'Arcy-Gall, R. D. Twesten, and J. E. Greene
Department of Materials Science and the Frederick Seitz Materials Research Laboratory, University of Illinois, 104 South Goodwin Avenue, Urbana, Illinois 61801

(Received 29 August 2002; accepted 5 November 2002)

Compressively strained $Si_{0.7}Ge_{0.3}$ layers were grown on Si(001) by gas-source molecular beam epitaxy from Ge_2H_6/Si_2H_6 mixtures at 450 °C. The combination of the relatively low growth temperature and high steady-state hydrogen surface coverage, $\theta_H = 0.52$ monolayer, completely suppresses strain-induced roughening and provides extremely flat surfaces with root mean square widths $w < 1.5$ Å for fully coherent layers. These samples were used as the starting point to probe mechanisms that control misfit-dislocation-induced surface roughening (i.e., crosshatch) along 90°-rotated ⟨110⟩ directions. For film thicknesses t just larger than the critical value for misfit dislocation formation, $t_c \simeq 1000$ Å, surface roughness is dominated by single- and multiple-atomic-height steps generated by the motion of threading dislocations associated with interfacial misfits. The surface steps are preferential H desorption sites and the increase in total step length results in a decrease in θ_H on terraces as well as at step edges. The latter effect allows a higher adatom crossing probability at ascending steps, leading to the formation of periodic ridges in response to local strain fields associated with misfit dislocation clusters; w increases from 3.1 Å at $t = 1350$ Å (corresponding to strain relaxation R of 1%) to 27 Å at $t = 4400$ Å ($R = 78\%$). Simultaneously, the decrease in θ_H on terraces strongly affects film growth kinetics as the deposition rates increase from 10 Å min^{-1} with $t < t_c$ to $\simeq 60$ Å min^{-1} with $t \simeq 1400-4400$ Å. Overall, in films with $t \lesssim 1440$ Å ($R \lesssim 5\%$), crosshatch is due to surface steps that result from multiple misfit dislocations on single glide planes. At higher film thicknesses ($R = 22-78\%$), crosshatch becomes dominated by local strain-induced roughening and leads to periodic ridge formation. © *2003 American Institute of Physics.* [DOI: 10.1063/1.1533833]

I. INTRODUCTION

Smooth surfaces are required for the fabrication, through band gap engineering, of high-frequency planar fully strained $Si_{1-x}Ge_x/Si(001)$ heterostructure devices with enhanced hole[1] and electron[2] mobilities, whereas controlled and reproducible roughening forms the basis for novel devices based upon self-organized quantum dots and wires.[3] In both cases, a detailed understanding of surface roughening mechanisms and reaction paths is required. The two primary strain relaxation mechanisms during heteroepitaxial film growth are strain-induced surface roughening and the formation of misfit dislocations at the layer/substrate interface. Strain-induced roughening is favored by higher film/substrate lattice-constant mismatch and higher growth temperatures.[4,5] Tersoff and LeGoues[6] showed that the activation energy for strain-induced roughening decreases rapidly with an increase in misfit strain ε, varying as ε^{-4}. In contrast, the activation energy for dislocation nucleation and multiplication varies much more slowly with layer strain, yielding an ε^{-1} dependence.

Strain relaxation through the formation of misfit dislocations in group IV and III–V semiconductor heterostructures results in a surface roughening morphology termed "crosshatch" which consists of periodic surface ridges aligned along orthogonal ⟨110⟩ surface directions.[7–10] Two different, but related, models have been proposed for the formation of surface crosshatch. Lutz *et al.*[8] reported that for layer thicknesses up to ≃5000 Å, surface roughening of $Si_{0.85}Ge_{0.15}$ alloys grown on Si(001) at 560 °C by ultrahigh vacuum (UHV) chemical vapor deposition could be accounted for simply by the formation of 60° misfit dislocations at the SiGe/Si interface. Each misfit dislocation, which forms by glide on {111} planes, results in a surface step of height $0.5a_s$, where a_s is the bulk Si lattice constant (5.430 88 Å).[11] With an increase in film thickness, multiheight surface steps arise due to periodic arrays of dislocation pileups on a common glide plane. For 4000-Å-thick layers, Lutz *et al.* found that the linear number density of pileups is approximately 1.5 μm^{-1}.

Fitzgerald and co-workers[9,10] and others[12,13] have argued that crosshatch surface relief features have heights which are too large to be explained by dislocation-induced surface steps alone. They proposed that crosshatch is primarily due to surface roughening driven by local strain fields associated with the presence of misfit dislocations. Since the initial ob-

[a]Electronic mail: tspila@uiuc.edu
[b]Present address: Groupe de Recherche en Physique et Technologie des Couches Minces, Département de Génie Physique, École Polytechnique de Montréal, P.O. Box 6079, Station Center-Ville, Montréal, Québec H3C 3A7, Canada.

Downloaded 30 Jan 2003 to 130.126.102.122. Redistribution subject to AIP license or copyright, see http://ojps.aip.org/japo/japcr.jsp

servation of crosshatch as a function of film thickness depends upon experimental resolution, it is likely that both mechanisms contribute with the dominant one depending upon the film/substrate lattice constant mismatch, film thickness, and layer growth conditions.

We have recently shown that strain-induced surface roughening in fully coherent $Si_{0.7}Ge_{0.3}/Si(001)$ structures ($\varepsilon \simeq 1.2\%$) is kinetically limited during gas-source molecular-beam epitaxy (GS-MBE) from hydride precursors at temperatures $T_s \leqslant 500\,°C$.[14] In fact, strain-induced roughening is completely quenched at $T_s = 450\,°C$ due to a combination of the low growth temperature and the correspondingly high steady-state hydrogen coverage, $\theta_H = 0.52$ monolayer (ML),[14] resulting in low adatom ascending-step-crossing probabilities.

In this article, we present the results of an investigation of the mechanisms that control the formation of surface crosshatch during GS-MBE of strained $Si_{0.7}Ge_{0.3}$ layers on Si(001). The films were grown as a function of thickness t from Ge_2H_6/Si_2H_6 gas mixtures in the surface-reaction-limited regime at $T_s = 450\,°C$. These conditions were chosen in order to eliminate strain-induced roughening prior to the introduction of dislocations, thereby allowing us to focus on strain relaxation through crosshatch formation. The surfaces of fully coherent alloy layers are extraordinarily flat with root mean square widths $w < 1.5$ Å. We use a combination of atomic force microscopy (AFM), high-resolution reciprocal lattice maps (HRRLM), and plan-view and cross-sectional transmission electron microscopy (TEM and XTEM, respectively) to show that layers having thicknesses t just greater than the critical value t_c for forming misfit dislocations, $\simeq 1000$ Å, develop single- and multiple-height atomic steps on the surface due to the glide of misfit dislocations. With further deposition, the degree of film relaxation R and the surface width w increase rapidly from $R = 1\%$ with $w = 3.1$ Å at $t = 1350$ Å to $R = 78\%$ with $w = 27$ Å at $t = 4400$ Å as the surface develops $\langle 110 \rangle$ ridges that have symmetric cross sections and rounded tops, which expand both laterally and vertically. The film growth rate R_{SiGe}, 10 Å min^{-1} for film thicknesses up to t_c, rises dramatically to $\simeq 60$ Å min^{-1} following the initiation of strain relaxation. We attribute this to the increased total length L of step edges, which act as preferential H desorption sites, leading to a decrease in the average terrace H coverage and, thereby, an increase in R_{SiGe}. The corresponding decrease, due to higher L values, in hydrogen step-edge coverage contributes to ridge formation and increased surface roughness at $t > t_c$ through the resulting increase in adatom ascending-step crossing probabilities.

II. EXPERIMENTAL PROCEDURE

All $Si_{0.7}Ge_{0.3}(001)$ layers were grown in a multichamber UHV system, described in detail in Ref. 15, with a base pressure of 5×10^{-11} Torr. The system is equipped with the capability for *in situ* temperature-programmed desorption (TPD), reflection high-energy electron diffraction (RHEED), low-energy electron diffraction (LEED), electron energy loss spectroscopy (EELS), and Auger electron spectroscopy (AES). During film growth experiments, Si_2H_6 and Ge_2H_6 molecular beams, with incident fluxes of 2.1×10^{16} and 1.3×10^{15} $cm^{-2}\,s^{-1}$, were delivered to the substrate through individual directed tubular dosers.

The substrates were 0.5-mm-thick n-type Si(001) wafers ($n = 1-2 \times 10^{14}$ cm^{-3}) with a miscut of $\simeq 0.1°$ in the $\langle 110 \rangle$ direction. Initial cleaning consisted of solvent degreasing, multiple wet-chemical oxidation/etch cycles, and a 60 s etch in dilute (2%) HF.[15] The substrates were then exposed to an UV/ozone treatment to remove C-containing species[16] and introduced, through the sample-exchange chamber, into the deposition system where they were degassed at 600 °C for 4 h and then rapidly heated at 100 °C s^{-1} to 1100 °C for 1 min to desorb the oxide layer. The RHEED patterns of substrates subjected to this procedure were 2×1 with sharp Kikuchi lines. No residual C or O was detected by AES. Si(001) buffer layers, 3000 Å thick, were deposited at $T_s = 800\,°C$ prior to the growth of $Si_{0.7}Ge_{0.3}$ alloy layers at $T_s = 450\,°C$. The high-temperature buffer layers serve two purposes: they cover any remaining surface contamination while simultaneously providing a more uniform distribution of terrace lengths.[17]

Deposited alloy layer thicknesses t and compositions x were determined using a combination of Rutherford backscattering spectroscopy (RBS), x-ray reflectivity (XRR), high-resolution x-ray diffraction (HRXRD), and HRRLM. Reported values for t and x are accurate to within ± 5 Å and $\pm 0.3\%$, respectively. The RBS measurements were carried out using 2 MeV He^+ ions and the results analyzed with the RUMP simulation program.[18] A Bede HRXRD system operated with a Cu $K\alpha_1$ monochromatic beam ($\lambda = 1.540\,597$ Å) was used to obtain XRR scans which were fit based upon the Fresnel reflectivity formulation of Parratt.[19]

HRXRD measurements were performed in a Philips diffractometer with Cu $K\alpha_1$ radiation from a four-crystal Ge(220) monochromator which provides an angular divergence of <12 arcsec with a wavelength spread of $\Delta\lambda/\lambda \simeq 7 \times 10^{-5}$. ω–2θ overview scans (ω is the angle of incidence and θ is the Bragg diffraction angle) were obtained with a detector acceptance angle of $\simeq 2°$, while an additional two-crystal Ge(220) analyzer was placed between the sample and the detector (acceptance angle $\simeq 12$ arcsec) to obtain high-resolution scans and HRRLM about both the symmetric and asymmetric reflections. HRRLMs are generated from successive ω–2θ rocking curve scans starting at different initial values for ω.

$Si_{0.7}Ge_{0.3}(001)$ surface morphological evolution was investigated as a function of film thickness t by contact-mode atomic force microscopy. The AFM measurements were carried out in air using Digital Instruments Nanoscope II and Multimode microscopes with oxide-sharpened Si_3N_4 tips having radii of 50–400 Å. The images were linearly planarized to remove sample tilting effects during the measurements. Additional line-by-line leveling was performed on the smoothest samples to remove low-frequency vibrational noise.

Height–difference, $G(\rho) = \langle |h_j - h_i|^2 \rangle$, and height–height, $H(\rho) = \langle h_i h_j \rangle$, correlation functions, where h is the

Downloaded 30 Jan 2003 to 130.126.102.122. Redistribution subject to AIP license or copyright, see http://ojps.aip.org/japo/japcr.jsp

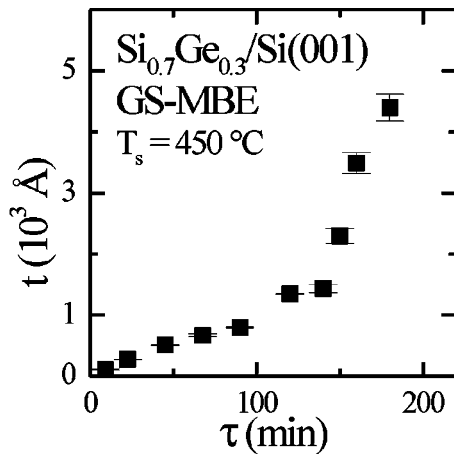

FIG. 1. Film thickness t as a function of deposition time τ during the growth of $Si_{0.7}Ge_{0.3}$ on Si(001) by hydride GS-MBE at $T_s = 450\,°C$.

height at positions i and j separated by a distance ρ and the angular brackets correspond to averages over the measured surface, were calculated from the AFM data. Values for the dominant in-plane length scale d are determined from the first maximum in $H(\rho)$, while values for the surface width w, which is equivalent to the root-mean-square roughness, are obtained using the relation $2w^2 = G(\rho) + 2H(\rho)$.

TEM and XTEM examinations were carried out using JEOL 2010F and Philips CM12 microscopes operated at 200 and 120 kV, respectively. Plan-view samples were prepared by thinning from the back side in a 10:1 HNO_3:HF solution. Specimens for XTEM examinations were prepared by mechanical thinning followed by ion milling as described in Ref. 20.

III. EXPERIMENTAL RESULTS

GS-MBE $Si_{0.7}Ge_{0.3}$ layers were grown to thicknesses ranging from 100 to 4400 Å on Si(001) at $T_s = 450\,°C$. The critical thickness t_c for misfit dislocation formation was determined from XTEM images (resolution in dislocation spacing $\simeq 1\ \mu m^{-1}$) and analyses of HRRLMs (resolution $\simeq 0.1\ \mu m^{-1}$) to be 1000 ± 200 Å. Ge surface segregation kinetics during the growth of fully coherent $Si_{0.7}Ge_{0.3}$/Si(001) layers by GS-MBE from hydride precursors have previously been determined as a function of T_s.[21] For the growth conditions used in the present experiments, steady-state Ge and H coverages θ_{Ge} and θ_H were found from isotopically tagged D_2 TPD measurements[22] to be 0.79 and 0.52 ML, respectively, for fully coherent layers.[21]

$Si_{0.7}Ge_{0.3}$(001) film thicknesses t as a function of deposition time τ (Ref. 23) are plotted in Fig. 1. For $t < t_c$, the film thickness increases approximately linearly with τ, corresponding to a deposition rate R_{SiGe} of 10 Å min^{-1}. The slope then changes rapidly to yield $R_{SiGe} \simeq 60$ Å min^{-1} over the thickness range between $\simeq 1400$ and 4400 Å. As discussed in Sec. IV, this suggests that the steady-state surface hydrogen coverage decreases at $t > t_c$.

Typical HRRLMs around asymmetric 113 reflections are shown in Fig. 2 for four $Si_{0.7}Ge_{0.3}$(001) layers of increasing thickness. Diffracted intensities are plotted as isointensity

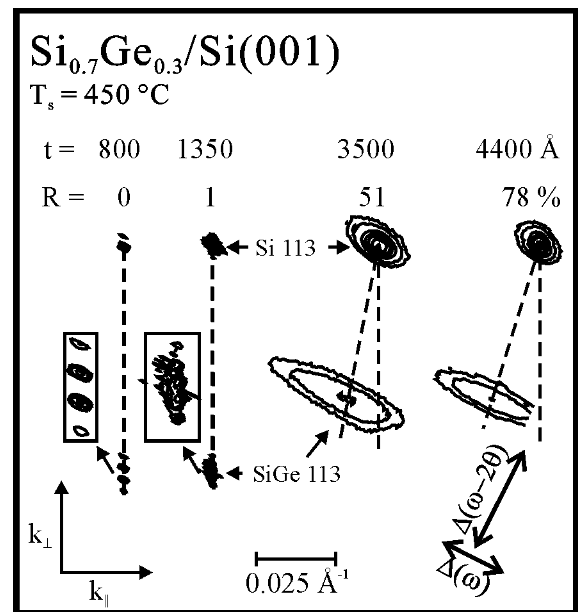

FIG. 2. HRRLMs around 113 Bragg peaks from $Si_{0.7}Ge_{0.3}$ layers grown on Si(001) by hydride GS-MBE at $T_s = 450\,°C$. The layer thickness t and degree of relaxation R are $t = 800$ Å, $R = 0$; $t = 1350$ Å, $R = 1\%$; $t = 3500$ Å, $R = 51\%$; and $t = 4400$ Å, $R = 78\%$. The insets next to the $t = 800$ and 1350 Å samples show details of the layer peaks.

contours as a function of the reciprocal lattice vectors $k_\parallel$ parallel and $k_\perp$ perpendicular to the surface. The substrate and layer scattering distributions are perfectly aligned (to within 10^{-5}) in the $k_\parallel$ direction for the 800 Å alloy, showing that the film is fully coherent with the substrate. The layer diffraction contours are nearly symmetric with no broadening in either the ω or $k_\parallel$ directions, an indication of high crystalline quality and low mosaicity. Finite-thickness interference fringes are visible and positioned periodically along the growth direction, consistent with the alloy layer being of high structural quality with a laterally uniform film/substrate interface. As the layer thickness increases, broadening in the ω and $k_\parallel$ directions is observed in both the substrate and layer peaks, suggesting larger surface and/or interface roughness with increased mosaicity. The position of the layer peak, with respect to that of the substrate, continuously shifts from being perfectly aligned along the $k_\perp$ direction toward being centered along the ω–2θ direction, which would correspond to complete strain relaxation.

$k_\parallel$ and $k_\perp$ in Fig. 2 are related to peak positions in ω–2θ space through the relationships[24]

$$k_\parallel = 2 r_E \sin(\theta)\cos(\omega - \theta) \tag{1}$$

and

$$k_\perp = 2 r_E \sin(\theta)\sin(\omega - \theta), \tag{2}$$

where r_E is the radius of the Ewald sphere given by $r_E = 1/\lambda = 0.649\,10$ Å^{-1}. For a 113 reflection from an 001-oriented diamond-structure crystal, the in-plane $a_\parallel$ and out-of-plane $a_\perp$ lattice constants are given by $a_\parallel = \sqrt{2}/k_\parallel$ and $a_\perp = 3/k_\perp$. The relaxed $Si_{0.7}Ge_{0.3}$ lattice constant a_0 is obtained from the relationship

Downloaded 30 Jan 2003 to 130.126.102.122. Redistribution subject to AIP license or copyright, see http://ojps.aip.org/japo/japcr.jsp

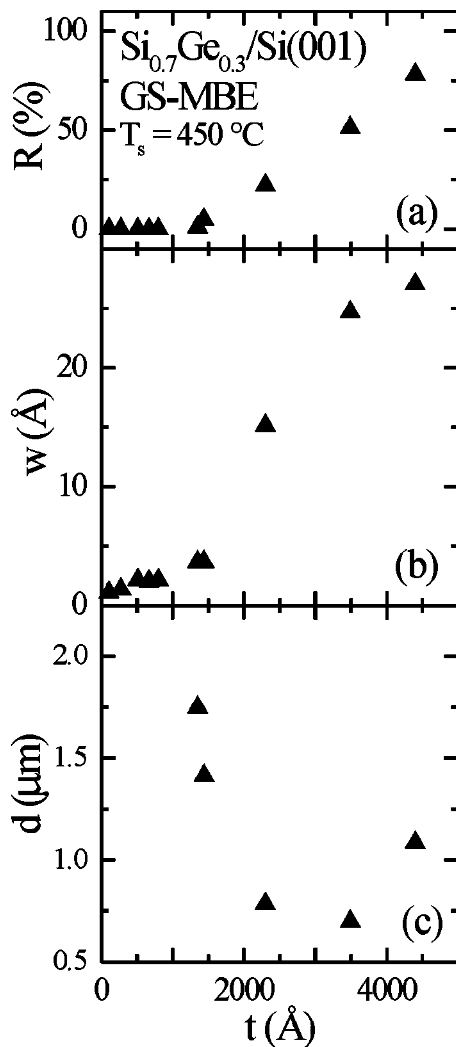

FIG. 3. (a) Strain relaxation R, (b) root-mean-square surface width w, and (c) average in-plane surface feature separation d as a function of the thickness t of $Si_{0.7}Ge_{0.3}$ layers grown on Si(001) by hydride GS-MBE at $T_s=450\,^{\circ}\mathrm{C}$.

$$a_0=a_\perp\left(1-\frac{2\nu(a_\perp-a_\parallel)}{a_\perp(1+\nu)}\right), \tag{3}$$

in which ν is the film Poisson ratio. The Ge fraction in the alloy layer is then determined from a_0 and linearly interpolated elastic constants using the corrections to Vegard's rule reported by Dismukes *et al.*[25] Measured values of $a_\parallel$ and $a_\perp$ are also used to determine the degree of in-plane layer relaxation R as

$$R=\frac{a_\parallel-a_s}{a_0-a_s}, \tag{4}$$

where a_s is the substrate lattice constant.[11] The Ge concentration for all layers, including the four presented in Fig. 2, is 0.30 ± 0.03, while the R values, plotted versus film thickness t in Fig. 3(a), range from $\simeq 0$ with $t<t_c$ (see, for example, the $t=800$ Å layer HRRLM in Fig. 2) to 78% for the $t=4400$ Å layer.

Figures 4 and 5 contain typical AFM images from layers grown to thicknesses below, above, and far above the critical thickness for the formation of misfit dislocations. Results for

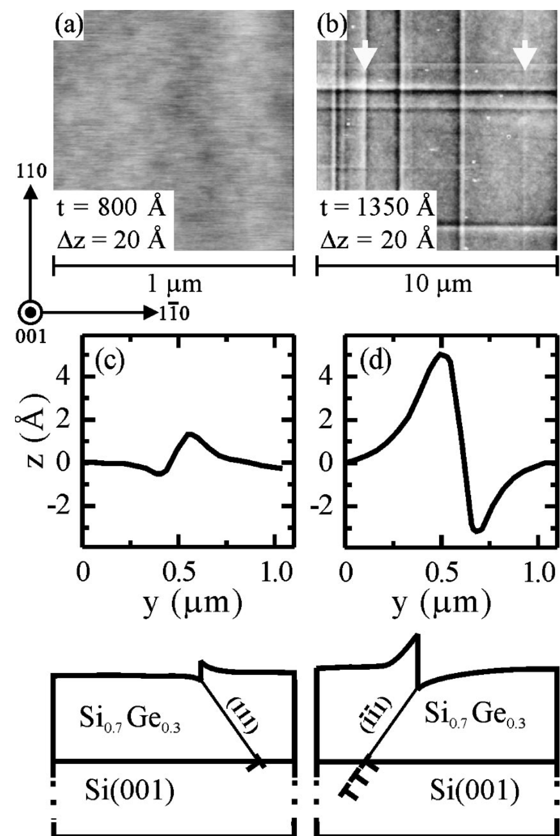

FIG. 4. AFM images from (a) 800-Å-thick and (b) 1350-Å-thick $Si_{0.7}Ge_{0.3}$ layers grown on Si(001) by hydride GS-MBE at $T_s=450\,^{\circ}\mathrm{C}$. (c), (d) AFM line scans over the single-height and triple-height dislocation-induced surface features indicated by the arrows on the right and the left, respectively, in (b). The lower panels are schematic cross-sectional diagrams corresponding to the sample regions shown in (c) and (d).

surface roughness and average in-plane feature separation as a function of the $Si_{0.7}Ge_{0.3}(001)$ film thickness are summarized in Figs. 3(b) and 3(c). All $Si_{0.7}Ge_{0.3}(001)$ films with thicknesses $t<t_c$ have smooth, flat surfaces with $w<1.5$ Å. An example is shown in Fig. 4(a) for the fully coherent 800-Å-thick layer in Fig. 2. The contrast in the AFM image is primarily due to vibrational noise.

Layers with t just larger than t_c remain highly strained with R varying only from 1% to 5% as t is increased from 1350 to 1440 Å. In this regime, the surface roughness is dominated by the formation of misfit-dislocation-induced surface steps with average feature heights which remain approximately constant and step–step separations d which decrease rapidly with an increase in film relaxation [see Fig. 3(c)]. At $t=1350$ Å, corresponding to a layer with $R=1\%$, the AFM image [Fig. 4(b)] exhibits long, straight surface steps which are aligned along orthogonal $\langle 110\rangle$ directions. The surface width and the average step-to-step separation are $w=3.1$ Å and $d=1.75$ μm, respectively.

Line scans across surface steps reveal that approximately half of the steps arise from single misfit dislocations with the remaining being multiheight and corresponding to up to four dislocations on a single slip plane. Sample line scans, which can be interpreted on the basis of associated schematic diagrams, are presented in Figs. 4(c) and 4(d) for single- and

Downloaded 30 Jan 2003 to 130.126.102.122. Redistribution subject to AIP license or copyright, see http://ojps.aip.org/japo/japcr.jsp

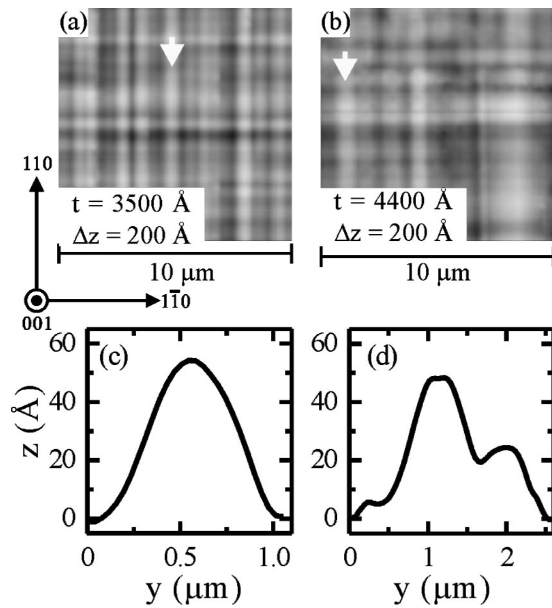

FIG. 5. AFM images from (a) 3500-Å-thick and (b) 4400-Å-thick $Si_{0.7}Ge_{0.3}$ layers grown on Si(001) by hydride GS-MBE at $T_s = 450\,°C$. (c), (d) AFM line scans over the surface features indicated by the arrows in (a) and (b), respectively.

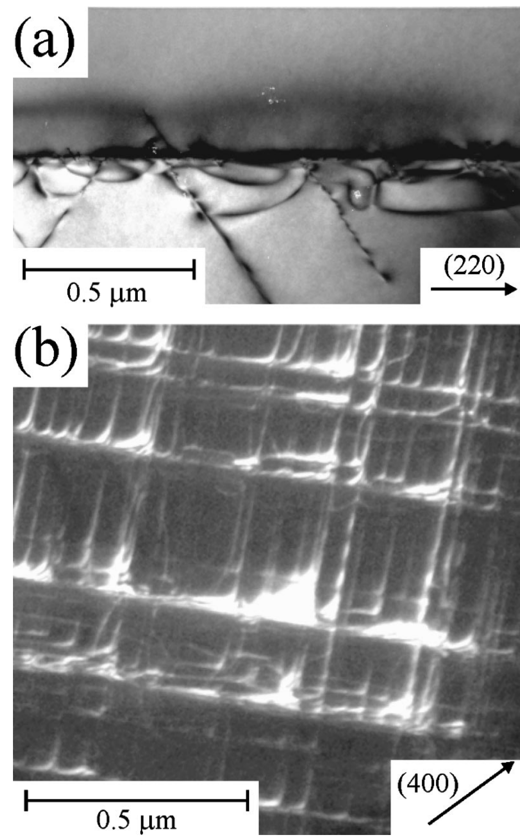

FIG. 6. (a) Bright-field 220 XTEM and (b) dark-field 004 plan-view TEM images of a $t = 4400$-Å-thick $Si_{0.7}Ge_{0.3}$ layer grown on Si(001) by hydride GS-MBE at $T_s = 450\,°C$.

triple-height steps. The single-height step [Fig. 4(c)] results from a 60° dislocation, indicated by the arrow on the right side of Fig. 4(b), with Burgers vector $\bar{b} = 0.5[101]$ at the intersection of a (111) glide plane and the film/substrate interface. In this case, the surface steps up toward the right. (Note that the screw component of the dislocation does not result in surface displacement.) Similarly, the surface feature shown in Fig. 4(d), which corresponds to the arrow on the left in Fig. 4(b), can be constructed from three dislocations with $\bar{b} = 0.5[011]$ on the same $(\bar{1}\bar{1}1)$ glide plane. The up step is toward the left. The asymmetric profiles of the steps, including the surface displacements on both sides of the step, can be accounted for by solution of the elasticity equations.[8]

The degree of film relaxation increases rapidly with $Si_{0.7}Ge_{0.3}(001)$ thickness $t \gtrsim 1440$ Å and the surface cross-hatch morphology continues to develop as shown in AFM images consisting of both dislocation-induced steps and periodic arrays of ridges along 90°-rotated ⟨110⟩ directions. However, with further increases in t, the surface morphology quickly becomes dominated by ridges. Figure 5(a) is an AFM image of a 3500-Å-thick layer for which $R = 51\%$. The ridges are approximately symmetric in cross section as shown by a typical line scan [Fig. 5(c)] across the feature labeled by the arrow in Fig. 5(a). The average surface width w of the ridges in this sample is 25 Å with an in-plane ridge-to-ridge spacing d of 7000 Å.

Figure 5(b) is an AFM image from a $t = 4400$-Å-thick layer with $R = 78\%$. Line profiles reveal that both the average height and width of the ridges in this layer are larger than those of the 3500-Å-thick film. A typical result is shown in Fig. 5(d) [note the change in lateral scale between Figs. 5(c) and 5(d)]. From an analysis of the image in Fig. 5(b), we obtain $w = 27$ Å with $d = 1.1\ \mu$m. The increase in ridge-to-ridge separation indicates that coalescence is occurring in these highly relaxed layers. This is clearly observed in Fig. 5(d) and consistent with the observation that the aspect ratio w/d of the ridges in the two thickest layers decreases slightly from 3.5 to 2.5×10^{-3} as t increases from 3500 to 4400 Å (see Fig. 3).

Figures 6(a) and 6(b) are XTEM and plan-view TEM images of the $t = 4400$ Å $Si_{0.7}Ge_{0.3}(001)$ sample which, from HRRLM measurements, is 78% relaxed. The $\bar{g} = 220$ bright-field XTEM micrograph shows the presence of misfit dislocations at the film/substrate interface as well as dislocation pileups that extend into the substrate along the (111) and $(\bar{1}\bar{1}1)$ glide planes. Pileups are also evident in the dark-field $\bar{g} = 400$ plan-view image that shows orthogonal dislocation arrays.

IV. DISCUSSION

$Si_{0.7}Ge_{0.3}(001)$ alloys grown on Si(001) at $T_s = 450\,°C$ from dihydride gas-phase precursors remain fully strained and commensurate with the substrate for film thicknesses t up to $t_c \simeq 1000$ Å. The layers have extremely flat surfaces with $w < 1.5$ Å. As t is increased above t_c, plastic shear displacement, associated with 60° dislocations gliding on {111} planes, results in the formation of surface steps of atomic dimensions. The roughness of $Si_{0.7}Ge_{0.3}(001)$ layers with thicknesses of 1350 and 1440 Å, corresponding to 1% and 5% relaxation, is dominated by these dislocation-induced surface steps. The AFM images consist of large flat

Downloaded 30 Jan 2003 to 130.126.102.122. Redistribution subject to AIP license or copyright, see http://ojps.aip.org/japo/japcr.jsp

terraces separated by long straight steps along orthogonal ⟨110⟩ directions as shown in Fig. 4(b). The step height associated with a single 60° dislocation is 2.7 Å. Multiheight steps are also observed due to multiple dislocations on a common glide plane.

Further increases in film thickness result in rapid strain relaxation through the introduction of additional misfit dislocations. At the same time, the overall film deposition rate increases dramatically and the surface morphology changes from being dominated by single- and multiheight ⟨110⟩ steps, giving rise to average surface widths w of $\simeq 3.1$ Å with $t = 1350-1440$ Å, to one consisting of orthogonal arrays of ⟨110⟩-oriented ridges with symmetric cross sections and $w = 25-27$ Å at $t = 3500-4400$ Å. We propose that both the onset of ridge formation, under growth conditions which quench strain-induced mound formation,[14] and the increase in R_{SiGe} are related to a decrease in surface H coverage with increasing in total step length.

Vasek *et al.*[26] have demonstrated, based upon scanning tunneling microscopy results, that small H coverages θ_H increase the activation energy E_s for diffusion of Si atoms on Si(001) terraces at $T_s \lesssim 250\,°C$. At higher T_s, however, the H atoms are sufficiently mobile that they have little effect on Si surface diffusion and E_s remains close to the value observed for clean Si(001). We expect similar results for dimers which are believed to be the primary diffusing species on Si(001),[27] and hence $Si_{1-x}Ge_x(001)$,[28] at the growth temperatures used in the present experiments.

While there are no reports on ad-dimer diffusion on Si(001) or $Si_{1-x}Ge_x(001)$ across step edges where H is present, first-principles total-energy calculations have shown that H increases the trap energy E_t for adatoms by $\simeq 0.1$ and 0.8 eV at S_A and S_B steps on Si(001).[29] Thus, while surface H has little effect on adatom mobilities, H atoms at step edges can significantly affect adatom ascending step-crossing probabilities during film growth. Two-dimensional surface segregation of H toward step edges, for which there is experimental evidence,[30] would serve to amplify this effect. The high steady-state hydrogen coverage during $Si_{0.7}Ge_{0.3}(001)$ GS-MBE at $T_s = 450\,°C$ contributes to the quenching of strain-induced mound formation, which, like ridge formation, requires uphill diffusion, by decreasing adatom ascending step-crossing rates.

Hydride GS-MBE $Si_{0.7}Ge_{0.3}(001)$ film growth kinetics are a complex function of the surface hydrogen coverage θ_H which, itself, depends on the Ge coverage θ_{Ge} through the strong θ_{Ge} dependence in the hydrogen desorption rates from surface Si and Ge sites.[31] In fact, the Ge segregation and hydrogen desorption rates are mutually dependent since the Ge segregation enthalpy decreases with an increase in θ_H.[20] The presence of hydrogen at Si surface sites not only reduces the surface energy, but directly decreases the Ge segregation rate through site blocking. In addition, the Si_2H_6 and Ge_2H_6 reactive sticking probabilities $S_{Si_2H_6}$ and $S_{Ge_2H_6}$ on Si and Ge sites also depend strongly on θ_H through θ_{Ge}.[20] By combining these results, it has been shown that $Si_{1-x}Ge_x(001)$ growth rates for fully strained layers are described well by the following expression:[20]

$$R_{SiGe} = \frac{2\theta_{Si} f_{db,Si}^2}{N_{SiGe}} (J_{Si_2H_6} S_{Si_2H_6}^{Si} + J_{Ge_2H_6} S_{Ge_2H_6}^{Si}) + \frac{2\theta_{Ge} f_{db,Ge}^2}{N_{SiGe}} (J_{Si_2H_6} S_{Si_2H_6}^{Ge} + J_{Ge_2H_6} S_{Ge_2H_6}^{Ge}) \quad (5)$$

$f_{db,Si}$ and $f_{db,Ge}$ in Eq. (5) are the fractional Si and Ge surface atom dangling bond coverages; the total dangling bond coverage $\theta_{db} = (1-\theta_H)$. J is the precursor flux while the terms S_p^s correspond to the reactive sticking probabilities of precursor p (Si_2H_6 or Ge_2H_6) at sites s (Si or Ge). Mixed dimers are ignored since their population fraction is less than 20% and the hydrogen desorption energy from mixed dimers is between that of Si and Ge dimers.[20]

$f_{db,Si}$ for $Si_{1-x}Ge_x(001)$ GS-MBE, in which Si_2H_6 adsorption and H_2 desorption are both second order, is given by[32]

$$f_{db,Si} = \left[1 + \sqrt{\frac{2 j_{Si_2H_6} S_{Si_2H_6}}{N_s \nu_s \exp\left(-\frac{E_{Si}(\theta_{Ge})}{kT_s}\right)}} \right]^{-1}. \quad (6)$$

N_s in Eq. (6) is the surface atom number density, ν_s is the H surface desorption prefactor, and $E_{Si}(\theta_{Ge})$ is the activation energy for H desorption from a Si surface site. $f_{db,Ge}$ is obtained from a parallel expression for Ge.

While $Si_{1-x}Ge_x(001)$ GS-MBE growth kinetics are far more complex, due to strong interactions among kinetic parameters, than those of Si(001)[33] [or Ge(001)][34,35] for which film growth rates are simply proportional to $(1-\theta_H)^2$, it is still clear from Eq. (5) that R_{SiGe} increases rapidly with a decrease in hydrogen coverage in the surface-reaction-limited regime.[20] This implies that the large increase we observe in $Si_{0.7}Ge_{0.3}(001)$ growth rates at $T_s = 450\,°C$ over the film thickness region corresponding to significant layer relaxation is due to a decrease in θ_H. We suggest that this occurs due to preferential H desorption from step edges as the total step edge length increases rapidly with film relaxation. Zhang *et al.*[30] reported a related observation. They found that the growth rate of Si(001) by GS-MBE from Si_2H_6 at $T_s = 500\,°C$ was higher on 4°-misoriented Si(001) than on nominally singular substrates.

In order to explain our $R_{SiGe}(t)$ results, we propose that the H desorption rate per site is only slightly larger at step edges than on terraces. This would result in a gradient in H coverage over a relatively narrow region ranging from step edges out onto adjacent terraces. Thus, for $Si_{1-x}Ge_x(001)$ surfaces with wide average terrace widths, the step edges have a negligible effect on the overall film growth rates. However, as the step densities increase with the formation of misfit dislocations, the terrace widths decrease and the H depleted zones around step edges become a significant source for reducing the average H coverage θ_H on terraces and, consequently, increasing R_{SiGe}. We estimate, based upon the average step separation due to dislocation-induced roughening, that for $Si_{0.7}Ge_{0.3}/Si(001)$ hydride GS-MBE at 450 °C, the total step edge length L initially increases slightly for film thicknesses between $\simeq 1000$ and 1440 Å, then increases by a factor of $\simeq 6\times$ as t is increased from 1440 to

Downloaded 30 Jan 2003 to 130.126.102.122. Redistribution subject to AIP license or copyright, see http://ojps.aip.org/japo/japcr.jsp

2300 Å and periodic ridges are formed. However, L remains approximately constant over the film thickness range from 2300 to 4400 Å due to the competition between ridge growth, which increases L, and ridge coalescence, which decreases L. Thus, we observe R_{SiGe} to initially increase dramatically at $t \simeq 1400$ Å, after which it remains approximately constant. We expect that R_{SiGe} will actually decrease at even higher thicknesses as ridge coalescence dominates and L decreases.

A decrease in θ_H resulting from misfit-dislocation-induced surface steps formed during $Si_{0.7}Ge_{0.3}(001)$ GS-MBE at $t > t_c$ not only increases R_{SiGe}, but also allows higher adatom ascending step-crossing rates, which is necessary for ridge growth via uphill mass transport driven by inhomogeneous strain fields around dislocations. Similar to the case of strain-induced roughening,[36] the overall behavior is controlled by two primary competing terms. The first, which corresponds to the surface free energy contribution to the chemical potential, depends on the curvature of the surface and tends to flatten the profile, while the second term is the elastic energy contribution which includes the strain fields around the dislocation cores and gives rise to a net flux of adatoms from valleys toward the ridges.

The local driving force for ridge formation initially increases with the creation of misfit dislocations, but then decreases with further increases in film thickness due to the growing distance between dislocation cores and the film surface. Thus, the slope of w vs t decreases at higher film thicknesses as shown in Fig. 3. At $t \gtrsim 3500$ Å, the ridge aspect ratio (w/d) decreases since $d(t)$, dominated by ridge coalescence, increases faster than $w(t)$.

Thus, the development of a crosshatch surface morphology in compressively strained $Si_{1-x}Ge_x/Si(001)$ layers occurs via an interactive combination of the two previously proposed mechanisms: slip steps and the growth of self-organized periodic ridges. Initially, the formation of misfit dislocations at the substrate/layer interface produces asymmetric surface steps along ⟨110⟩ directions. These additional surface steps act as preferential H desorption sites, thereby increasing the film growth rate while promoting adatom migration across ascending steps. Uphill adatom diffusion, driven by the strain fields associated with the dislocations leads to the formation of symmetrically shaped ⟨110⟩ ridge structures.

V. CONCLUSIONS

We have shown that surface hydrogen mediates both film growth kinetics and the evolution of misfit dislocation-induced surface roughness through interactions with step edges during hydride GS-MBE of compressively strained $Si_{0.7}Ge_{0.3}$ layers on Si(001) at $T_s = 450\,°C$. The film growth conditions were chosen such that the competing mechanism for surface roughening, strain-induced mound formation, was totally quenched. Layers with thicknesses t less than the critical value for the formation of misfit dislocations, $t_c \simeq 1000$ Å, remain flat with surface widths $w < 1.5$ Å. This results from a combination of the relatively low growth temperature and the correspondingly high steady-state hydrogen coverage during growth ($\theta_H = 0.52$ ML) and gives rise to low adatom ascending step-crossing rates.

At layer thicknesses $t > t_c$, the glide of misfit dislocations along {111} planes produces single- and multiheight surface steps along orthogonal ⟨110⟩ directions. The surface steps act as preferential H desorption sites; thus, the dislocation-induced increased total step length leads to a decrease in θ_H on terraces and, therefore, an increase in R_{SiGe}. The corresponding decrease in the hydrogen concentration at step edges enhances uphill surface mass transport, which is driven by large inhomogeneous strain fields around dislocation clusters, over ascending steps and leads to the formation of ridges, with symmetric cross sections, which increase in height and width with an increase in film relaxation. Thus, both of the previously proposed mechanisms for crosshatch formation are observed with contributions which vary with the film thickness.

For film thicknesses just greater than t_c, the degree of film relaxation and the increase in step density remain relatively low. The average step separation d varies from 1.75 μm at $R = 1\%$ ($t = 1350$ Å) to 1.4 μm at $R = 5\%$ ($t = 1440$ Å) while the average feature height, $w \simeq 3.1$ Å, remains approximately constant. This gives rise to only a modest, although measurable, increase in R_{SiGe}. At higher film thicknesses, the surface morphology is composed of a combination of dislocation-induced surface steps and ridges with the ridges dominating the observed crosshatch as t increases. w ranges from 15 Å at $t = 2300$ Å ($R = 22\%$) to 25 Å at $t = 3500$ Å ($R = 51\%$) to 27 Å at $t = 4400$ Å ($R = 78\%$) while R_{SiGe}, 10 Å min^{-1} at $t < t_c$, increases to $\simeq 60$ Å min^{-1} over the thickness range from 1400 to 4400 Å. The large increase in R_{SiGe} is associated with a decrease in θ_H due to the rapid increase in step length L at film thicknesses between $\simeq 1400$ and 2300 Å. L, and hence R_{SiGe}, then remains approximately constant at higher film thicknesses (2300–4400 Å) due to the competition between ridge growth and coalescence.

ACKNOWLEDGMENTS

The authors gratefully acknowledge the financial supported of the U.S. Department of Energy, Division of Materials Sciences, under Award No. DEFG02-ER9645439 and the NSF Focused Research Group on Nanoscale Morphological Control of Strained Semiconductor Surfaces, Grant No. DMR-0075116, during the course of this research. Some experiments were carried out in the Center for Microanalysis of Materials, University of Illinois, which is partially supported by the U.S. Department of Energy under Grant No. DEFG02-91-ER45439. One of the authors (P.D.) was partially supported by the Natural Sciences and Engineering Research Council (NSERC) of Canada and the Fonds pour la Formation de Chercheurs et l'Aide à la Recherche (FCAR) of Québec, Canada.

[1] Q. Lu, M. R. Sardela, Jr., T. R. Bramblett, and J. E. Greene, J. Appl. Phys. **80**, 4458 (1996).
[2] G. Abstreiter, H. Brugger, T. Wolf, H. Jorke, and H. J. Herzog, Phys. Rev. Lett. **54**, 2441 (1985).
[3] P. M. Petroff and G. Medeiros-Ribeiro, MRS Bull. **21**, 50 (1996).

Downloaded 30 Jan 2003 to 130.126.102.122. Redistribution subject to AIP license or copyright, see http://ojps.aip.org/japo/japcr.jsp

[4] N. E. Lee, M. Matsuoka, M. R. Sardela, Jr., F. Tian, and J. E. Greene, J. Appl. Phys. **80**, 812 (1996).
[5] N. E. Lee, D. G. Cahill, and J. E. Greene, J. Appl. Phys. **80**, 2199 (1996).
[6] J. Tersoff and F. K. LeGoues, Phys. Rev. Lett. **72**, 3570 (1994).
[7] S. Y. Shiryaev, F. Jensen, and J. W. Petersen, Appl. Phys. Lett. **64**, 3305 (1994).
[8] M. A. Lutz, R. M. Feenstra, F. K. LeGoues, P. M. Mooney, and J. O. Chu, Appl. Phys. Lett. **66**, 724 (1995).
[9] E. A. Fitzgerald, Y. H. Xie, D. Monroe, P. J. Silverman, J. M. Kuo, A. R. Kortan, F. A. Thiel, and B. E. Weir, J. Vac. Sci. Technol. B **10**, 1807 (1992).
[10] J. W. P. Hsu, E. A. Fitzgerald, Y. H. Xie, P. J. Silverman, and M. J. Cardillo, Appl. Phys. Lett. **61**, 1293 (1992).
[11] Powder Diffraction Card No. 27-1402, JCPDS-International Center for Diffraction Data, Newton Square, PA (1997).
[12] T. Pinnington, C. Lavoie, T. Tiedje, B. Haveman, and E. Nodwell, Phys. Rev. Lett. **79**, 1698 (1997).
[13] T. Pinnington, C. Lavoie, and T. Tiedje, J. Vac. Sci. Technol. B **15**, 1265 (1997).
[14] T. Spila, P. Desjardins, A. Vailionis, H. Kim, N. Taylor, D. G. Cahill, J. E. Greene, S. Guillon, and R. A. Masut, J. Appl. Phys. **91**, 3579 (2002).
[15] Q. Lu, T. R. Bramblett, N. E. Lee, M. A. Hasan, T. Karasawa, and J. E. Greene, J. Appl. Phys. **77**, 3067 (1995).
[16] X. J. Zhang, G. Xue, A. Agarwal, R. Tsu, M. A. Hasan, J. E. Greene, and A. Rockett, J. Vac. Sci. Technol. A **11**, 2553 (1993).
[17] P. Desjardins and J. E. Greene, J. Appl. Phys. **79**, 1423 (1996).
[18] L. R. Doolittle, Nucl. Instrum. Methods Phys. Res. B **9**, 344 (1985).
[19] L. G. Parratt, Phys. Rev. **95**, 359 (1954).
[20] J. P. Noel, N. Hirashita, L. C. Markert, Y. W. Kim, J. E. Greene, J. Knall, W. X. Ni, M. A. Hasan, and J. E. Sundgren, J. Appl. Phys. **65**, 1189 (1989).
[21] H. Kim, N. Taylor, T. R. Bramblett, and J. E. Greene, J. Appl. Phys. **84**, 6372 (1998).
[22] H. Kim, N. Taylor, J. R. Abelson, and J. E. Greene, J. Appl. Phys. **82**, 6062 (1997).
[23] In order to provide comparable data for samples with both smooth and rough surfaces, all thickness values reported here were obtained from XRR and RBS measurements of the total atom density per unit area and therefore correspond to the nominal thickness of smooth layers grown under the specified set of deposition conditions.
[24] P. van der Sluis, J. Phys. D **26**, A188 (1993).
[25] J. P. Dismukes, L. Ekstrom, and R. J. Paff, J. Phys. Chem. **68**, 3021 (1964).
[26] J. E. Vasek, Z. Zhang, C. T. Salling, and M. G. Lagally, Phys. Rev. B **51**, 17207 (1995).
[27] M. Krueger, B. Borovsky, and E. Ganz, Surf. Sci. **385**, 146 (1997).
[28] X. R. Qin, B. S. Swartzentruber, and M. G. Lagally, Phys. Rev. Lett. **85**, 3660 (2000).
[29] S. Jeong and A. Oshiyama, Phys. Rev. Lett. **81**, 5366 (1998).
[30] J. Zhang, A. K. Lees, A. G. Taylor, M. H. Xie, B. A. Joyce, Z. Sobiesierkski, and D. I. Westwood, J. Cryst. Growth **175–176**, 477 (1997).
[31] H. Kim, P. Desjardins, J. R. Abelson, and J. E. Greene, Phys. Rev. B **58**, 4803 (1998).
[32] H. Kim, G. Glass, T. Spila, N. Taylor, S. Y. Park, J. R. Abelson, and J. E. Greene, J. Appl. Phys. **82**, 2288 (1997).
[33] T. R. Bramblett, Q. Lu, T. Karasawa, M. A. Hasan, S. K. Jo, and J. E. Greene, J. Appl. Phys. **76**, 1884 (1994).
[34] H. Kim and J. E. Greene, J. Vac. Sci. Technol. A **17**, 354 (1999).
[35] T. R. Bramblett, Q. Lu, N. E. Lee, N. Taylor, M. A. Hasan, and J. E. Greene, J. Appl. Phys. **77**, 1504 (1995).
[36] D. E. Jesson, S. J. Pennycook, J.-M. Baribeau, and D. C. Houghton, Phys. Rev. Lett. **71**, 1744 (1993).

Downloaded 30 Jan 2003 to 130.126.102.122. Redistribution subject to AIP license or copyright, see http://ojps.aip.org/japo/japcr.jsp